Frontiers in Heat and Mass Transfer (FHMT), 20, 23 (2023)
DOI: 10.5098/hmt.20.23

Global Digital Central
ISSN: 2151-8629

Frontiers in Heat and Mass Transfer

Available at www.ThermalFluidsCentral.org

# ANALYTICAL SOLUTION OF THE EXTENDED GRAETZ PROBLEM IN MICROCHANNELS AND MICROTUBES WITH FIXED PRESSURE DROP

Mohamed Shaimi*, Rabha Khatyr, Jaafar Khalid Naciri

*Laboratory of Mechanics, Faculty of Sciences Aïn Chock, Hassan* II *University of Casablanca, Casablanca,* 20100*, Morocco*

## ABSTRACT

This paper presents an exact analytical solution to the extended Graetz problem in microchannels and microtubes, including axial heat conduction, viscous dissipation, and rarefaction effects for an imposed constant wall temperature. The flow in the microchannel or microtube is assumed to be hydrodynamically fully developed. At the same time, the first-order slip-velocity and temperature jump models represent the wall boundary conditions. The energy equation is solved analytically, and the solution is obtained in terms of Kummer functions with expansion constants directly determined from explicit expressions. The local and fully developed Nusselt numbers are calculated in terms of the Péclet number, Brinkman number, Knudsen number, and thermal properties of the fluid. The constant pressure drop along the streamwise direction per unit length is imposed at a constant value and independent of the flow parameters, unlike the usual practice of fixing the average velocity. This solution can be used as the reference solution for optimization problems to enhance heat transfer using a fixed pressure drop. It is found that for no viscous dissipation and negligible axial heat conduction, the local Nusselt number is larger for imposed pressure drop compared to imposed average velocity. The thermal entrance length increases as the Knudsen number or the degree of temperature jump increases for imposed pressure drop, while it is approximately unchangeable for imposed average velocity. The quantitative differences between the cases of imposed pressure drop and imposed average velocity in the average Nusselt number over the largest thermal entrance length are reduced with the increase of axial heat conduction or viscous dissipation effects. The fully developed Nusselt number is the same for imposed pressure drop and imposed average velocity.

**Keywords**: *Axial Heat Conduction, Viscous Dissipation, Slip Flow, Constant Wall Temperature, Temperature Jump.*

## 1. INTRODUCTION

The miniaturization of industrial products is continuously evolving due to the technological development in many industrial fields. The ever-increasing miniaturization raises several challenges in which cooling plays an important role, such as in the development of micro-heat-exchangers (Chung et *al.*, 2011; Khan and Fartaj, 2011; Han et *al.*, 2012; Ismail et *al.*, 2012; Kanor and Manimaran, 2016; Zhang, 2017; Qasem and Zubair, 2018; Zarita and Hachemi, 2019; Ramesh *et al.*, 2021; Soheel et *al.*, 2021; Turkyilmazoglu, 2021b; Gao *et al.*, 2022; Gulia and Sur, 2022; Al-Gburi et *al.*, 2023; Jaddoa et *al.*, 2023). Therefore, understanding the physics of heat transfer and fluid flow at the microscale level has a significant role in this industrial trend. Microelectromechanical systems (MEMS) have characteristic lengths between 1 $mm$ and 1 $\mu m$. The Knudsen number $Kn = \lambda/L_c$ compares the mean free path $\lambda$ to the characteristic length of the flow $L_c$, which is used to classify different flow regimes. According to Beskok and Kamiadakis (1994) and Gad-el-Hak (1999) and following empirical information, the fluid can be considered as a continuum for $Kn \leq 10^{-3}$, which is known as the no-slip flow, the slip flow is for $10^{-3} < Kn < 0.1$ and the transition flow for $0.1 < Kn < 10$, while for $Kn \geq 10$ it is considered free molecular flow. In microfluidics, Navier-Stokes and energy equations can still be used to predict the slip flows and early transition flows; however, there are corrections to the boundary conditions that have to be made by taking into consideration the slip-velocity and the temperature jump at the walls.

This paper focuses on the analytical study of the fluid flow and heat transfer in microchannels and microtubes to investigate the effects of the axial heat conduction, viscous dissipation, and rarefaction on the heat transfer for the slip flow regime corresponding to $10^{-3} < Kn < 0.1$. The microchannel or microtube is considered infinite. The boundary conditions at the walls are divided into two regions with two different values of the constant wall temperature. The junction point is the abscise of the step change in the wall temperature. The usual uniform inlet temperature condition is not used due to the effects of axial heat conduction and viscous dissipation. The main interest of this study is to consider a fixed pressure drop along the streamwise direction per unit length as opposed to the heavily studied usual case of fixed average velocity. Let us note that the case studied in this paper is of significant importance and can be useful for optimization problems or energy efficiency maximization (Fabbri, 2000; Tian et *al.*, 2022), such as in electronic components cooling, where the pumping power is important.

In the case of no-slip flow, the Graetz problem, which is the steady laminar incompressible thermally developing and hydrodynamically developed flow in a tube with Dirichlet boundary condition, was first studied by Graetz (1882). The inlet temperature is considered uniform due to the hypotheses of negligible viscous dissipation and axial heat conduction, which leads to the parabolic form of the energy equation, where only the inlet condition and the wall boundary conditions are needed to obtain the solution in the channel or tube. The results and conclusions are the same either a fixed average velocity is used or a fixed pressure drop along the streamwise direction per unit length due to the linear relationship between them, which is given by the Hagen-Poiseuille equation. Shah and London (1978) reviewed various analytical and

* *Corresponding author. Email: mohamed.shaimi-etu@etu.univh2c.ma*

Global Digital Central
ISSN: 2151-8629

numerical methods used to solve the Graetz problem in different macroscale configurations, including the effects of axial heat conduction and viscous dissipation. The extended Graetz problem, which includes axial heat conduction, has been studied by many researchers (Hennecke, 1968; Papoutsakis *et al.*, 1980; Lahjomri and Oubarra, 1999). Hennecke (1968) found that a uniform inlet temperature assumption is not justified for small Péclet numbers due to the upstream effect related to axial heat conduction. Recently, Turkyilmazoglu (2021a) studied the extended Graetz problem analytically in parallel-plate channels with a moving upper wall and a fixed lower wall where the simple Couette flow gives the considered hydrodynamically developed flow. It was found that the heat transfer rate at the moving wall is of significant importance as the Péclet number increases. Viscous dissipation and axial heat conduction effects on the fully developed forced convection of non-Newtonian fluids were investigated analytically by Khatyr and Khalid Naciri (2022).

The viscous dissipation effect on the Graetz problem is known to be important for the slip flow in microchannels or microtubes. Sparrow and Lin (1962) studied the Graetz problem analytically under slip flow conditions. It was found that for a constant average velocity, the Nusselt number decreases with increasing the Knudsen number and the rate of reduction is influenced by the degree of temperature jump. The thermal entrance length also increases as the Knudsen number increases. Larrodé *et al.* (2000) studied the influence of rarefaction on heat transfer in microtubes. They introduced a spatial rescaling factor, which measures rarefaction through its dependence on the Knudsen number to identify similarities with the classical Graetz problem. Tunc and Bayazitoglu (2001) studied the Graetz problem in microtubes, including slip flow, temperature jump, and viscous dissipation, using the integral transform technique. For a fixed average velocity, it was found that as the Prandtl number increases, the temperature jump effect diminishes, which leads to an increase in the Nusselt number. Xu *et al.* (2003) studied the effects of viscous dissipation in microchannel flows to provide evidence for the assumption that, at the microscale, viscous dissipation could be too important to be neglected. Rosa *et al.* (2009) reviewed the importance of scaling effects for single-phase heat transfer in microchannels. Recently, Turkyilmazoglu (2022) studied analytically the thermal performance of optimum exponential fins subjected to a temperature jump at the base. It was found that the temperature jump's overall effect on the fin efficiency is such that it works to reduce the fin efficiency.

Many investigations studied the coupling of axial heat conduction, viscous dissipation, and rarefaction effects on the Graetz problem in microchannels and microtubes, and to the best of our knowledge, all of them used the fixed average velocity condition (Jeong and Jeong, 2006; Çetin *et al.*, 2008; Çetin and Zeinali, 2014; Barişik *et al.*, 2015; Kalyoncu and Barişik, 2016; Haddout *et al.*, 2020; Sun *et al.*, 2020). However, for optimization problems or energy efficiency maximization, the variation of the pressure drop along the streamwise direction per unit length in the microchannel or microtube is as important as the variation of the Nusselt number. Therefore, the heat transfer result, Nusselt number, is limited by not considering the change in the pressure drop along the streamwise direction per unit length. Jeong and Jeong (2006) used the hypothesis of a uniform inlet temperature. Çetin *et al.* (2008) show that the fully developed Nusselt number and the thermal entrance length increase with the decrease of the Péclet number. Çetin and Zeinali (2014) used a second-order slip model to model the rarefaction effects. The temperature distribution, the Nusselt number, and the entropy generation are calculated in terms of confluent hypergeometric functions. They identified that for a negligible viscous dissipation, the Nusselt number decreases as the Knudsen number increases and decreases when the modeling is changed from the first-order model with negligible terms at $Kn^2$ to the second-order model. For a non-negligible viscous dissipation, the Nusselt number predicted by the first-order model is lower than that predicted by the second-order model. Barişik *et al.* (2015) and Kalyoncu and Barişik (2016) used the Gram-Schmidt orthogonalization technique (Dutta *et al.*, 2006) due to the use of a uniform inlet temperature hypothesis. Barişik *et al.* (2015) concluded that for all cases with negligible viscous dissipation and short tubes with viscous dissipation, the axial heat conduction should not be neglected for Péclet numbers less than 100. For large length-over-diameter ratios, the viscous dissipation effect should be considered even for small Brinkman numbers. Kalyoncu and Barişik (2016) found that the convective heat transfer coefficient increases with decreasing flow dimensions despite the reduction of the Nusselt number. Haddout *et al.* (2020) used the self-adjoint formalism method involving the decomposition of the energy equation into a system of two first-order partial differential equations. It was concluded that heat transfer increases as the Péclet number and the Knudsen number decrease; at the same time, for large Péclet numbers, the Knudsen number does not affect the temperature gradient near-wall layer, while for small Péclet numbers, this effect becomes important. Sun *et al.* (2020) used the Gram-Schmidt orthogonalization procedure with the Gauss-Legendre quadrature due to the uniform inlet temperature hypothesis. It was found that the effect of the axial heat conduction on the fully developed Nusselt number is negligible for Péclet numbers greater than 10. In contrast, its effect on the Nusselt number and the bulk temperature can be neglected only for Péclet numbers greater than 100.

The objective of this paper is to study the flow parameters' effects on the extended Graetz problem in microchannels and microtubes with axial heat conduction, viscous dissipation, slip flow, and temperature jump by using an exact analytical solution. The first-order slip-velocity and temperature jump models are used, and the fixed constant pressure drop along the streamwise direction per unit length condition is considered. Therefore, the results of the effects of the Knudsen number and the degree of temperature jump on heat transfer are presented differently from those found in the case of a fixed average velocity condition (Larrodé *et al.*, 2000; Tunc and Bayazitoglu, 2001; Jeong and Jeong, 2006; Çetin *et al.*, 2008; Çetin and Zeinali, 2014; Barişik *et al.*, 2015; Kalyoncu and Barişik, 2016; Haddout *et al.*, 2020; Sun *et al.*, 2020). The obtained analytical solution is directly applied without introducing the spatial rescaling factor (Larrodé *et al.*, 2000), which is used for a fixed average velocity. Additionally, the results in the case of average velocity can be found by using the relationship between the pressure drop along the streamwise direction per unit length and the average velocity to redefine the dimensionless numbers. The temperature is written as a superposition of the fully developed temperature and an expansion in terms of a complete set which leads to an eigenvalue problem where the eigenfunctions are given by Kummer functions, and the expansion constants are determined by using a similar procedure to that presented by Lahjomri and Oubarra (1999). The Nusselt number is calculated for different values of the flow parameters to investigate their effects on heat transfer in both cases of imposed pressure drop along the streamwise direction per unit length and imposed average velocity.

This paper is organized into five sections. The second section presents the analysis with the geometrical configuration, the mathematical formulation, and the analytical solution. The third section is devoted to the validation of the proposed analytical solution with the literature. Then, the fourth section presents the results and discussions. Finally, the last section presents the main conclusions of this research.

## 2. ANALYSIS

### 2.1 Geometrical Configuration

Figure 1 shows the geometrical configuration of the considered microchannel or microtube. The parallel plate microchannel is symmetric, and the cylindrical microtube is axisymmetric, including the distribution of the boundary conditions, and as long as no force breaks the symmetry of the equations derived from the conservation laws, then only a part of the microchannel or microtube can be studied by adding a symmetry condition at the centerline. The distance between the centerline and the wall, $d$, is half the height for a microchannel and the radius for a microtube. The variable $\eta^*$ represents the transversal coordinate for a microchannel and the radial coordinate for a microtube.

Global Digital Central
ISSN: 2151-8629

The variable $x^*$ is the longitudinal coordinate. The constant wall temperature is $T_{w1}$ for $x^* < 0$ and $T_{w2}$ for $x^* > 0$. The junction point at $x^* = 0$ represents the abscise of the step change in the wall temperature. The flow is supposed to be fully developed at $x^* = -\infty$, where the developed velocity and temperature profiles are respectively given by $u^*(\eta^*)$ and $T^*_{-\infty}(\eta^*)$, and at $x^* = +\infty$, where the developed velocity and temperature profiles are respectively given by $u^*(\eta^*)$ and $T^*_{+\infty}(\eta^*)$.

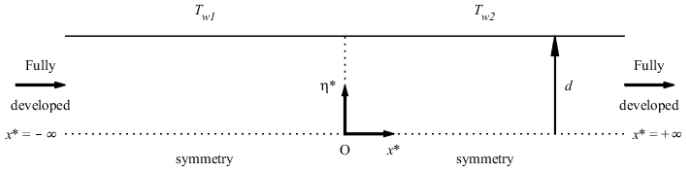


**Fig. 1** The geometrical configuration of the considered microchannel or microtube.

## 2.2 Mathematical Formulation

Using the previously introduced assumptions, the governing equations for mass and momentum conservation reduce to the following system (Shah and London, 1978):

$$\frac{\partial u^*}{\partial x^*} = 0 \tag{1}$$

$$\frac{1}{\eta^{*l}}\frac{\partial}{\partial \eta^*}\left(\eta^{*l}\frac{\partial u^*}{\partial \eta^*}\right) = \frac{1}{\mu}\frac{\partial p^*}{\partial x^*} \tag{2}$$

$$\frac{\partial p^*}{\partial \eta^*} = 0 \tag{3}$$

where $l$ is a geometrical parameter that accepts two values, $l = 0$ represents the microchannel case, and $l = 1$ represents the microtube. The constant pressure gradient along the streamwise direction is $\frac{dp^*}{dx^*}$ (Shah and London, 1978). $u^*$, $p^*$ and $\mu$ are respectively the velocity component in the $x^*$-direction, pressure, and dynamic viscosity of the fluid. $(x^*, \eta^*)$ are the cartesian coordinates for a microchannel and the cylindrical coordinates for a microtube.

The slip-velocity (Beskok and Karniadakis, 1994; Gad-el-Hak, 1999) at the stationary wall of the microchannel or microtube is given by:

$$u^*(\eta^* = d) = -\frac{2-\sigma_v}{\sigma_v}\lambda\left.\frac{du^*}{d\eta^*}\right|_{\eta^*=d} \tag{4}$$

where $\lambda$ and $\sigma_v$ are respectively the mean free path of the molecules and the tangential momentum accommodation coefficient.

The symmetry condition for the velocity at the centerline is given by:

$$\left.\frac{du^*}{d\eta^*}\right|_{\eta^*=0} = 0 \tag{5}$$

Integrating Eq. (2) and using the boundary conditions, Eqs. (4) and (5), lead to the velocity distribution, which is written as follows:

$$u^*(\eta^*) = -\frac{d^2}{2(l+1)\mu}\frac{dp^*}{dx^*}\left[1 - \left(\frac{\eta^*}{d}\right)^2 + 2\frac{2-\sigma_v}{\sigma_v}\frac{\lambda}{d}\right] \tag{6}$$

The energy equation with the axial heat conduction and viscous dissipation is given by (Shah and London, 1978):

$$\rho C_p u^*(\eta^*)\frac{\partial T_j^*}{\partial x^*} = k\left(\frac{\partial^2 T_j^*}{\partial x^{*2}} + \frac{1}{\eta^{*l}}\frac{\partial}{\partial \eta^*}\left(\eta^{*l}\frac{\partial T_j^*}{\partial \eta^*}\right)\right) + \mu\left(\frac{du^*}{d\eta^*}\right)^2 \tag{7}$$

where $C_p$, $k$, $\rho$ and $T_j^*$ are respectively the specific heat, the thermal conductivity, the density, and the temperature of the fluid. The index $j$ represents two regions with two different wall temperature values where $j = 1$ for $x^* < 0$ and $j = 2$ for $x^* > 0$.

The temperature jump (Beskok and Karniadakis, 1994; Gad-el-Hak, 1999) at the wall of the microchannel or microtube is given by:

$$T_j^*(x^*, \eta^* = d) - T_{wj} = -\frac{2-\sigma_T}{\sigma_T}\frac{2\gamma}{\gamma+1}\frac{\lambda}{Pr}\left.\frac{\partial T_j^*}{\partial \eta^*}\right|_{\eta^*=d} \tag{8}$$

where $\sigma_T$ is the energy accommodation coefficient, $Pr = \frac{\mu C_p}{k}$ is the Prandtl number, and $\gamma$ is the specific heat ratio. $T_{wj}$ is the wall temperature where $j = 1$ for $x^* < 0$ and $j = 2$ for $x^* > 0$.

The symmetry condition for the temperature at the centerline is given by:

$$\left.\frac{\partial T_j^*}{\partial \eta^*}\right|_{\eta^*=0} = 0 \tag{9}$$

The condition for the temperature respectively at $x^* = -\infty$ and $x^* = +\infty$ are given by:

$$T_1^*(x^* = -\infty, \eta^*) = T^*_{-\infty}(\eta^*) \tag{10}$$

$$T_2^*(x^* = +\infty, \eta^*) = T^*_{+\infty}(\eta^*) \tag{11}$$

The flow is considered to be fully developed far upstream at $x^* = -\infty$ and far downstream at $x^* = +\infty$. Therefore, $T^*_{-\infty}(\eta^*)$ and $T^*_{+\infty}(\eta^*)$ are independent of the axial coordinate $x^*$ even for small Péclet numbers due to their large distance from the junction point at $x^* = 0$ where the axial heat conduction can play a significant role. Note that for a negligible viscous dissipation, the fluid temperature far upstream and far downstream are respectively the corresponding wall temperatures of each region, $T_{w1}$ and $T_{w2}$ (Lahjomri and Oubarra, 1999) with no temperature jump due to the null temperature gradient at the walls of the microchannel or microtube far upstream and far downstream, Eq. (8). However, in the presence of viscous dissipation, they are dependent on the variable $\eta^*$ and their expressions will be given later using the energy equation along with the wall boundary conditions.

The temperature and the axial heat flux are continuous at the section of the step change in the wall temperature $x^* = 0$. Therefore, the additional continuity conditions at the junction section $x^* = 0$ are given by:

$$T_1^*(x^* = 0, \eta^*) = T_2^*(x^* = 0, \eta^*) \text{ for } 0 \le \eta^* < d \tag{12}$$

$$\left.\frac{\partial T_1^*}{\partial x^*}\right|_{x^*=0} = \left.\frac{\partial T_2^*}{\partial x^*}\right|_{x^*=0} \tag{13}$$

Defining the dimensionless variables as follows:

$$x = \frac{x^*}{d\cdot Pe};\quad \eta = \frac{\eta^*}{d};\quad u = \frac{u^*}{\frac{d^2}{2(l+1)\mu}\Delta p_L^*} = 1 - \eta^2 + 2^{3-l}\frac{2-\sigma_v}{\sigma_v}Kn;$$

$$T_j = \frac{T_j^* - T_{w2}}{T_{w1} - T_{w2}} \tag{14}$$

where $\Delta p_L^* = -\frac{dp^*}{dx^*} = \text{constant}$ is the pressure drop along the streamwise direction per unit length, which is positive due to the negative pressure gradient along the streamwise direction, $Pe = \frac{\rho C_p d^3}{2(l+1)\mu k}\Delta p_L^*$ is the Péclet number, $Kn = \frac{\lambda}{D_h}$ is the Knudsen number, and $D_h = 2^{2-l}d$ is the hydraulic diameter for the microchannel $(l = 0)$ and the microtube $(l = 1)$. The dimensionless temperature in Eq. (14) is written in a form similar to that used in (Lahjomri and Oubarra, 1999).

By using parameters of Eq. (14), the dimensionless energy equation becomes:

$$u(\eta)\frac{\partial T_j}{\partial x} = \frac{1}{Pe^2}\frac{\partial^2 T_j}{\partial x^2} + \frac{1}{\eta^l}\frac{\partial}{\partial \eta}\left(\eta^l\frac{\partial T_j}{\partial \eta}\right) + Br\left(\frac{du}{d\eta}\right)^2 \tag{15}$$

Global Digital Central
ISSN: 2151-8629

where $Br = \frac{d^4(\Delta p_L^*)^2}{4(l+1)^2\mu k(T_{w1}-T_{w2})}$ is the Brinkman number that accounts for the viscous dissipation effect.

The dimensionless boundary conditions become:

$$T_1(x,\eta=1) = 1 - 2^{2-l}\,\kappa\, Kn \frac{\partial T_1}{\partial \eta}\Big|_{\eta=1} \quad (16)$$

$$T_2(x,\eta=1) = -2^{2-l}\,\kappa\, Kn \frac{\partial T_2}{\partial \eta}\Big|_{\eta=1} \quad (17)$$

$$\frac{\partial T_j}{\partial \eta}\Big|_{\eta=0} = 0 \quad (18)$$

$$T_1(x=-\infty,\eta) = T_{-\infty}(\eta) \quad (19)$$

$$T_2(x=+\infty,\eta) = T_{+\infty}(\eta) \quad (20)$$

$$T_1(x=0,\eta) = T_2(x=0,\eta) \text{ for } 0 \le \eta < 1 \quad (21)$$

$$\frac{\partial T_1}{\partial x}\Big|_{x=0} = \frac{\partial T_2}{\partial x}\Big|_{x=0} \quad (22)$$

where $\kappa = \frac{2-\sigma_T}{\sigma_T}\frac{2\gamma}{\gamma+1}\frac{1}{Pr}$ is a parameter that accounts for the degree of temperature jump and $T_{\mp\infty} = \frac{T^*_{\mp\infty}-T_{w2}}{T_{w1}-T_{w2}}$ are the dimensionless temperatures far upstream and far downstream given by (see Appendix A):

$$T_{-\infty}(\eta) = 1 + \frac{Br}{3+l}(1-\eta^4 + 2^{4-l}\,\kappa\, Kn) \quad (23)$$

$$T_{+\infty}(\eta) = \frac{Br}{3+l}(1-\eta^4 + 2^{4-l}\,\kappa\, Kn) \quad (24)$$

The solutions of Eq. (15) are sought as a superposition in the following form:

$$T_j(x,\eta) = T_{\mp\infty}(\eta) + \Theta_j(x,\eta) \quad (25)$$

where $\Theta_j(x,\eta)$ are unknown functions introduced due to the step change in the wall temperature at the junction point, and they vanish far upstream and far downstream.

Substituting Eq. (25) into the energy equation, Eq. (15), and since $T_{\mp\infty}(\eta)$ satisfies the energy equation, one obtains:

$$u(\eta)\frac{\partial \Theta_j}{\partial x} = \frac{1}{Pe^2}\frac{\partial^2 \Theta_j}{\partial x^2} + \frac{1}{\eta^l}\frac{\partial}{\partial \eta}\left(\eta^l \frac{\partial \Theta_j}{\partial \eta}\right) \quad (26)$$

With the following boundary conditions on the functions $\Theta_j(x,\eta)$:

$$\Theta_j(x,\eta=1) = -2^{2-l}\,\kappa\, Kn \frac{\partial \Theta_j}{\partial \eta}\Big|_{\eta=1} \quad (27)$$

$$\frac{\partial \Theta_j}{\partial \eta}\Big|_{\eta=0} = 0 \quad (28)$$

$$\Theta_1(x=-\infty,\eta) = 0 \quad (29)$$

$$\Theta_2(x=+\infty,\eta) = 0 \quad (30)$$

$$1 + \Theta_1(x=0,\eta) = \Theta_2(x=0,\eta) \text{ for } 0 \le \eta < 1 \quad (31)$$

$$\frac{\partial \Theta_1}{\partial x}\Big|_{x=0} = \frac{\partial \Theta_2}{\partial x}\Big|_{x=0} \quad (32)$$

## 2.3 Analytical Solution

The solutions of Eq. (26) for $j = 1$ and 2 are written as expansions in terms of a complete set in the following forms (Lahjomri and Oubarra, 1999):

$$\Theta_1(x,\eta) = \sum_n A_n f_n(\eta) e^{\alpha_n^2 x} \quad (33)$$

$$\Theta_2(x,\eta) = \sum_n B_n g_n(\eta) e^{-\beta_n^2 x} \quad (34)$$

where Eqs. (29) and (30) are satisfied accordingly. $A_n$ and $B_n$ are the expansion constants, $\alpha_n$ and $\beta_n$ are the real eigenvalues respectively associated with the eigenfunctions $f_n(\eta)$ and $g_n(\eta)$ that are respectively determined using the following equations:

$$\frac{d}{d\eta}\left(\eta^l \frac{df_n}{d\eta}\right) + \alpha_n^2\left[\frac{\alpha_n^2}{Pe^2} - (1-\eta^2+\varepsilon)\right]\eta^l f_n(\eta) = 0 \quad (35)$$

$$\frac{d}{d\eta}\left(\eta^l \frac{dg_n}{d\eta}\right) + \beta_n^2\left[\frac{\beta_n^2}{Pe^2} - (1-\eta^2+\varepsilon)\right]\eta^l g_n(\eta) = 0 \quad (36)$$

With the following boundary conditions:

$$f_n(\eta=1) = -\delta \frac{df_n}{d\eta}\Big|_{\eta=1} \quad (37)$$

$$\frac{df_n}{d\eta}\Big|_{\eta=0} = 0 \quad (38)$$

$$g_n(\eta=1) = -\delta \frac{dg_n}{d\eta}\Big|_{\eta=1} \quad (39)$$

$$\frac{dg_n}{d\eta}\Big|_{\eta=0} = 0 \quad (40)$$

where $\varepsilon = 2^{3-l}\frac{2-\sigma_v}{\sigma_v}Kn$ and $\delta = 2^{2-l}\,\kappa\, Kn$.

Introducing the following new variables and functions:

$$\chi = i\alpha_n\eta^2 \quad (41)$$

$$\psi_n(\chi) = e^{\frac{\chi}{2}} f_n(\eta) \quad (42)$$

$$\xi = \beta_n\eta^2 \quad (43)$$

$$\phi_n(\xi) = e^{\frac{\xi}{2}} g_n(\eta) \quad (44)$$

where $i^2 = -1$.

Substituting Eqs. (41)-(44) into Eqs. (35) and (36), yield the following known equations:

$$\chi\frac{d^2\psi_n}{d\chi^2} + (c-\chi) - a_n\psi_n(\chi) = 0 \quad (45)$$

$$\xi\frac{d^2\phi_n}{d\xi^2} + (c-\xi) - b_n\phi_n(\xi) = 0 \quad (46)$$

where $c = \frac{1+l}{2}$, $a_n = \frac{1+l}{4} - \frac{i+\varepsilon}{4}\alpha_n + \frac{i\alpha_n^3}{4Pe^2}$, and $b_n = \frac{1+l}{4} - \frac{1+\varepsilon}{4}\beta_n - \frac{\beta_n^3}{4Pe^2}$.

The solutions of Eqs. (45) and (46) are expressed in terms of the confluent hypergeometric functions. Therefore, considering that the eigenfunctions $f_n(\eta)$ and $g_n(\eta)$ are continuous for $0 < \eta < 1$, they are written as follows:

$$f_n(\eta) = e^{-\frac{i\alpha_n\eta^2}{2}} M(a_n, c, i\alpha_n\eta^2) \quad (47)$$

$$g_n(\eta) = e^{-\frac{\beta_n\eta^2}{2}} M(b_n, c, \beta_n\eta^2) \quad (48)$$

where $M$ is the Kummer confluent first-kind hypergeometric function.

The eigenvalues $\alpha_n$ and $\beta_n$ can be calculated, using the boundary conditions Eqs. (37) and (39), respectively as the roots of the equations $f_n(\eta=1) + \delta\frac{df_n}{d\eta}\Big|_{\eta=1} = 0$ and $g_n(\eta=1) + \delta\frac{dg_n}{d\eta}\Big|_{\eta=1} = 0$. To determine the expansion constants $A_n$ and $B_n$, the conditions at the junction section, Eqs. (31) and (32), are used. Substituting Eqs. (33) and (34) into Eqs. (31) and (32) lead to the following equations:

$$1 + \sum_n A_n f_n(\eta) = \sum_n B_n g_n(\eta) \text{ for } 0 \le \eta < 1 \quad (49)$$

$$\sum_n \alpha_n^2 A_n f_n(\eta) = -\sum_n \beta_n^2 B_n g_n(\eta) \quad (50)$$

Noting that the eigenfunctions $f_n(\eta)$ and $g_n(\eta)$ satisfy the following properties:

$$\int_0^1 \left(\frac{\alpha_n^2+\alpha_m^2}{Pe^2} - (1-\eta^2+\varepsilon)\right)\eta^l\, f_n(\eta) f_m(\eta) d\eta \begin{cases} = 0 & if \quad m \ne n \\ \ne 0 & if \quad m = n \end{cases} \quad (51)$$

$$\int_0^1 \left(\frac{\beta_n^2+\beta_m^2}{Pe^2} + (1-\eta^2+\varepsilon)\right)\eta^l\, g_n(\eta) g_m(\eta) d\eta \begin{cases} = 0 & if \quad m \ne n \\ \ne 0 & if \quad m = n \end{cases} \quad (52)$$

Global Digital Central
ISSN: 2151-8629

As well as the following boundary conditions:

$$f_n(\eta=1)\left.\frac{dg_m}{d\eta}\right|_{\eta=1} = g_m(\eta=1)\left.\frac{df_n}{d\eta}\right|_{\eta=1} = -\delta\left.\frac{df_n}{d\eta}\right|_{\eta=1}\left.\frac{dg_m}{d\eta}\right|_{\eta=1} \quad (53)$$

Following a similar procedure to that presented by Lahjomri and Oubarra (1999), the expansion constants $A_n$ and $B_n$ are calculated by using the following expressions:

$$A_n = -\frac{\int_0^1\left[\frac{\alpha_n^2}{Pe^2}-(1-\eta^2+\varepsilon)\right]\eta^l f_n(\eta)d\eta}{\int_0^1\left[\frac{2\alpha_n^2}{Pe^2}-(1-\eta^2+\varepsilon)\right]\eta^l [f_n(\eta)]^2 d\eta} \quad (54)$$

$$B_n = \frac{\int_0^1\left[\frac{\beta_n^2}{Pe^2}+(1-\eta^2+\varepsilon)\right]\eta^l g_n(\eta)d\eta}{\int_0^1\left[\frac{2\beta_n^2}{Pe^2}+(1-\eta^2+\varepsilon)\right]\eta^l [g_n(\eta)]^2 d\eta} \quad (55)$$

To avoid the heavy calculations due to the integrals in Eqs. (54) and (55), the following expressions for the expansion constants presented by Haddout *et al.* (2020) can be used:

$$A_n = \frac{2}{\alpha_n\left[\frac{df_n(\eta=1)}{d\alpha_n}+\delta\frac{d}{d\alpha_n}\left(\left.\frac{df_n}{d\eta}\right|_{\eta=1}\right)\right]} \quad (56)$$

$$B_n = -\frac{2}{\beta_n\left[\frac{dg_n(\eta=1)}{d\beta_n}+\delta\frac{d}{d\beta_n}\left(\left.\frac{dg_n}{d\eta}\right|_{\eta=1}\right)\right]} \quad (57)$$

The derivations in Eqs. (56) and (57) are calculated only once, in general, for an unknown eigenvalue then the different eigenvalues are replaced to find the associated expansion constant. The comparison between the values found by using Eqs. (54) and (55) with those found by using Eqs. (56) and (57) for different values of the dimensionless numbers is presented in Appendix B and shows that they are in perfect agreement in the no-slip flow regime (Table B.1). In the presence of a slip-velocity and temperature jump, the results are also in perfect agreement in the downstream region while they differ slightly in the upstream region for the first eigenvalues (Table B.2). The difference in the values of the expansion constants in the upstream region does not affect the results obtained in the downstream region which is the region of interest.

The local Nusselt number is calculated for the region where there is a change in the wall temperature $x > 0$ as follows:

$$Nu(x) = \frac{q_w D_h}{k\left(T_{w2}-T_b^*(x^*)\right)} = \frac{-2^{2-l}\left.\frac{\partial T_2}{\partial \eta}\right|_{\eta=1}}{T_b(x)} \quad (58)$$

where $q_w = k\left.\frac{\partial T_2^*}{\partial \eta^*}\right|_{\eta^*=d}$ is the heat flux at the walls for $x > 0$, $T_b^*(x^*)$ is the dimensional bulk temperature, and $T_b(x) = \frac{T_b^*(x^*)-T_{w2}}{T_{w1}-T_{w2}}$ is the dimensionless bulk temperature which is given by the following equation:

$$T_b(x) = \frac{\int_0^1 u(\eta)\, T_2(x,\eta)\, \eta^l\, d\eta}{\int_0^1 u(\eta)\, \eta^l\, d\eta} \quad (59)$$

The average velocity is written as follows:

$$U_{ave} = \frac{\int_0^1 \frac{d^2}{2(l+1)\mu}\Delta p_L^* u(\eta)\eta^l d\eta}{\int_0^1 \eta^l d\eta} = \frac{d^2}{2(l+1)\mu}\Delta p_L^*\left(\frac{2}{l+3}+2^{3-l}\frac{2-\sigma_v}{\sigma_v}Kn\right) \quad (60)$$

Equation (60) shows that the average velocity is proportional to the pressure drop along the streamwise direction per unit length. However, the slope is dependent on the Knudsen number and the tangential momentum accommodation coefficient. As in the Nusselt number Eq. (58), the velocity appears explicitly only in the bulk temperature Eq. (59) in both the numerator and denominator. For the case of $Kn = 0$, the results are similar either a fixed average velocity is chosen, or a fixed pressure drop along the streamwise direction per unit length. Otherwise, for $Kn \neq 0$, the results are not the same due to the dependence of the slope on the Knudsen number Eq. (60). Thus, the results are presented differently in the literature (Larrodé *et al.*, 2000; Tunc and Bayazitoglu, 2001; Jeong and Jeong, 2006; Çetin *et al.*, 2008; Çetin and Zeinali, 2014; Barişik *et al.*, 2015; Kalyoncu and Barişik, 2016; Haddout *et al.*, 2020; Sun *et al.*, 2020) for the case of an average velocity independent of the flow parameters being chosen as the characteristic velocity. This paper focuses on the case of a pressure drop along the streamwise direction per unit length independent of the flow parameters. However, Eq. (60) can be used to obtain the Péclet number, Brinkman number, the dimensionless longitudinal coordinate, and the dimensionless velocity distribution in terms of the average velocity instead of the pressure drop along the streamwise direction per unit length and therefore find the results presented in the literature.

## 3. VALIDATION

This section is devoted to the validation of the presented analytical procedure and the calculations done by comparing the results with literature data obtained using various analytical and numerical methods for different values of the dimensionless numbers.

### 3.1 No-slip Flow Regime Case with Axial Heat Conduction

In the no-slip flow regime, $Kn = 0$, the results found by using a fixed pressure drop along the streamwise direction per unit length are identical to those found by a fixed average velocity due to the proportionality that relates them, Eq. (60), with a slope independent of the dimensionless numbers. Therefore, the presented analytical solution can be compared for a fixed pressure drop along the streamwise direction per unit length with literature data for a fixed average velocity. Lahjomri and Oubarra (1999) studied the extended Graetz problem analytically in a channel or a tube with a step change in the wall temperature. They presented a general procedure for the direct determination of the expansion constants and presented the results in the case of the Hagen-Poiseuille flow. Barişik *et al.* (2015) investigated the extended Graetz problem analytically in microtubes, including axial heat conduction, viscous dissipation, and rarefaction effects by using the Gram-Shmidt orthogonalization technique and a uniform inlet temperature. Using a uniform inlet temperature in a semi-infinite microtube or an upstream region in an infinite microtube leads to different results in the thermal entrance or thermally developing region. However, the results in the fully developed region are identical due to their independence of the temperature profile at the inlet (Barişik *et al.*, 2015) or the junction section (present study). Table 1 shows a comparison of the fully developed Nusselt number $Nu_{FD}$ and the first eigenvalue $\beta_1$ in a tube ($l = 1$) for different Péclet numbers, $Br = 0$, and $Kn = 0$ with the results of Lahjomri and Oubarra (1999) and Barişik *et al.* (2015) for negligible viscous dissipation and rarefaction effects. It is shown that they are in perfect agreement. $Nu_{FD}$ decreases with the increase of $Pe$.

**Table 1** Comparison of the fully developed Nusselt number and the first eigenvalue in a tube for different Péclet numbers and $Br = 0$ with the literature.

| $Pe$ | | 1 | 2 | 5 | 10 | 50 | 100 | 1000 | $10^6$ |
|---|---|---|---|---|---|---|---|---|---|
| $Nu_{FD}$ | Present study | 4.02735 | 3.92236 | 3.76729 | 3.69518 | 3.65858 | 3.65724 | 3.65680 | 3.65679 |
| | Lahjomri and Oubarra (1999) | 4.02735 | 3.92236 | 3.76729 | 3.69518 | 3.65858 | 3.65724 | 3.65680 | 3.65679 |
| | Barişik *et al.* (2015) | 4.02735 | 3.92236 | 3.76729 | 3.69518 | 3.65858 | 3.65724 | 3.65680 | 3.65679 |
| $\beta_n$ | Present study | 1.42981 | 1.86755 | 2.38530 | 2.59693 | 2.69945 | 2.70313 | 2.70435 | 2.70436 |
| | Lahjomri and Oubarra (1999) | 1.42981 | 1.86755 | 2.38530 | 2.59693 | 2.69945 | 2.70313 | 2.70435 | 2.70436 |
| | Barişik *et al.* (2015) | 1.42981 | 1.86754 | 2.38530 | 2.59693 | 2.69945 | 2.70313 | 2.70435 | 2.70436 |

### 3.2 No-slip Flow Regime Case with Axial Heat Conduction and Viscous Dissipation

Sphaier *et al.* (2021) presented an analytical solution for the extended Graetz problem with axial heat conduction, viscous dissipation, and additional volumetric heating effects in a channel or a tube via the generalized integral transform technique. Four combinations of boundary conditions are studied where the walls of the upstream region are either isothermal or thermally insulated, and the walls of the downstream region are either isothermal or uniformly heated with a step change in the boundary condition at the junction point. Figs. 2(a) and 2(b) show the evolution of $Nu$ as a function of $x$ in a tube $(Kn = 0; l = 1)$ for $Pe = 1, 2, 10$ and respectively $Br = 0$ and $Br = 0.4$. The results agree with those of Sphaier *et al.* (2021) for $N = 1000$ and negligible volumetric heating effects with small quantitative differences in the thermal entrance region due to the different analytical techniques used to obtain these results. For no viscous dissipation $Br = 0$, the local Nusselt number increases with the decrease of the Péclet number for all the values of $x$. In the presence of viscous dissipation, the fully developed Nusselt number is independent of the Péclet number.

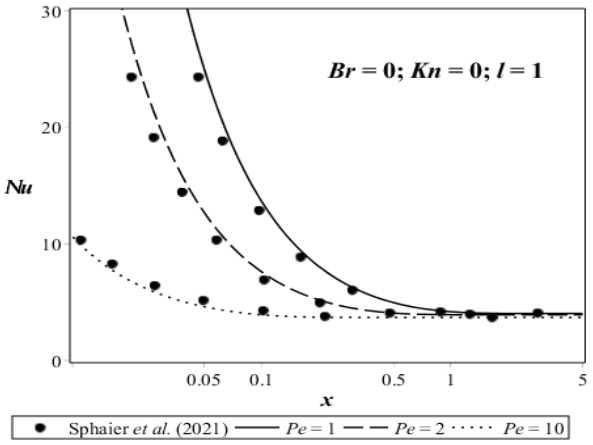


(a) $Br = 0$

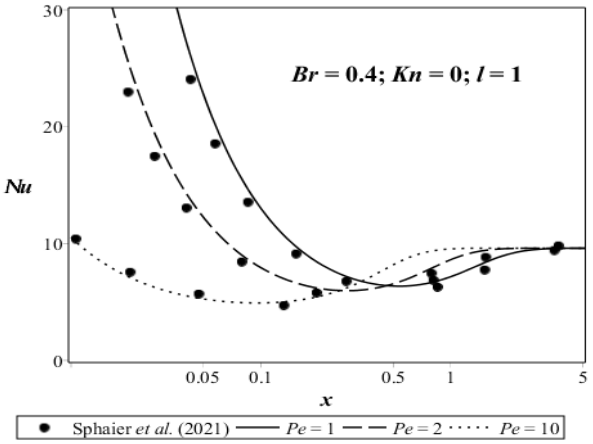


(b) $Br = 0.4$

**Fig. 2** Evolution of the local Nusselt number as a function of $x$ in a tube for different Péclet numbers as well as a comparison with the results of Sphaier *et al.* (2021) considering both cases of: (a) no viscous dissipation and (b) viscous dissipation.

### 3.3 Slip Flow Regime Case with Imposed Average Velocity

In contrast, for the case of the slip flow regime, $Kn \neq 0$, the slope coefficient that relates the pressure drop along the streamwise direction per unit length to the average velocity, Eq. (60), is dependent on the Knudsen number. Therefore, to validate the presented methodology with literature data, a fixed average velocity is considered by using similar characteristic parameters as Barişik *et al.* (2015) in a microtube $(l = 1)$ and using a similar procedure to that presented in this paper to determine the eigenvalues, expansion constants, and the Nusselt number. Çetin *et al.* (2008) studied the extended Graetz problem in microtubes with axial heat conduction, viscous dissipation, and rarefaction. The velocity profile is determined analytically, while the temperature distribution is obtained by a numerical solution of the energy equation based on the finite difference technique. Table 2 shows a comparison of the fully developed Nusselt number $Nu_{FD}$ in a microtube $(l = 1)$ for different Péclet numbers $Pe = 1, 2, 5, 10, 1000$, Knudsen numbers $Kn = 0.4, 0.8$, and degrees of temperature jump, $\sigma_v = 1$ and $Br = 0$ with the results of Çetin *et al.* (2008) and Barişik *et al.* (2015). The results are in good agreement with the literature data. They show that $Nu_{FD}$ increases as the Knudsen number increases for the case of no-temperature-jump at the walls $(\kappa = 0)$, while in the case of the temperature jump at the walls, $Nu_{FD}$ decreases with the increase of the Knudsen number or the degree of temperature jump, $\kappa$.

**Table 2** Comparison of the fully developed Nusselt number in a microtube for different Péclet numbers, Knudsen numbers, and degrees of temperature jump, $\sigma_v = 1$, and $Br = 0$ with the literature using a fixed average velocity.

| $\kappa$ | $Kn$ | $Pe$ | $Nu_{FD}$ | | |
|---|---|---|---|---|---|
| | | | Present study | Çetin *et al.* (2008) | Barişik *et al.* (2015) |
| 0 | 0.04 | 1 | 4.353 | 4.358 | ---- |
| | | 2 | 4.262 | 4.270 | ---- |
| | | 5 | 4.124 | 4.131 | ---- |
| | | 10 | 4.057 | 4.061 | ---- |
| | | 1000 | 4.021 | 4.020 | ---- |
| | 0.08 | 1 | 4.577 | 4.585 | ---- |
| | | 2 | 4.499 | 4.509 | ---- |
| | | 5 | 4.376 | 4.386 | ---- |
| | | 10 | 4.314 | 4.319 | ---- |
| | | 1000 | 4.279 | 4.279 | ---- |
| 1.667 | 0.04 | 1 | 3.597 | 3.604 | 3.603 |
| | | 2 | 3.509 | 3.517 | 3.517 |
| | | 5 | 3.380 | 3.387 | 3.387 |
| | | 10 | 3.322 | 3.325 | 3.325 |
| | | 1000 | 3.292 | 3.292 | 3.292 |
| | 0.08 | 1 | 3.087 | 3.093 | 3.093 |
| | | 2 | 3.028 | 3.036 | 3.035 |
| | | 5 | 2.943 | 2.949 | 2.949 |
| | | 10 | 2.906 | 2.909 | 2.908 |
| | | 1000 | 2.887 | 2.887 | 2.886 |
| 10 | 0.04 | 1 | 1.704 | 1.706 | ---- |
| | | 2 | 1.676 | 1.678 | ---- |
| | | 5 | 1.642 | 1.643 | ---- |
| | | 10 | 1.629 | 1.630 | ---- |
| | | 1000 | 1.624 | 1.624 | ---- |
| | 0.08 | 1 | 1.028 | 1.029 | ---- |
| | | 2 | 1.020 | 1.021 | ---- |
| | | 5 | 1.011 | 1.012 | ---- |
| | | 10 | 1.009 | 1.009 | ---- |
| | | 1000 | 1.008 | 1.008 | ---- |

These comparisons, carried out by considering the cases where the average velocity is imposed, show that the proposed solution achieves the same results as those usually obtained for laminar forced convection and thus ensures the reliability of the proposed approach.

### 3.4 Accuracy Analysis

Figures 3(a) and 3(b) show the evolution of the local Nusselt number $Nu$ as a function of the dimensional longitudinal coordinate $x$ for $Pe = 5$, $Br = 0$, and $Kn = 0$ respectively in a tube $(l = 1)$ and a channel $(l = 0)$. These figures show a comparison with the results of Lahjomri and Oubarra (1999) in the case of no-slip flow and no viscous dissipation hypotheses and exemplify the effect of the truncation order $N$ on the accuracy of $Nu$ for small values of $x$. The results of $Nu$ for $N = 250$ and $N = 300$ are identical in the range of $x \geq 0.001$ presented in Figs. 3(a) and 3(b). Due to the step change in the wall temperature, a higher value of $N$ is needed to find accurate results near the junction point. As the truncation order gets smaller, the local Nusselt number near the junction point is underpredicted. In this work, the results are limited to $x \geq 0.01$ in the following section, and $N = 50$ is used. However, as can be seen in Figs. 3(a) and 3(b), the results are accurate for $x \geq 0.01$ with $N = 50$. Although the results are quantitatively different for small values of $x$ and the different values of $N$, they are qualitatively similar. For $N = 20$, the results are in perfect agreement with those of Lahjomri and Oubarra (1999).

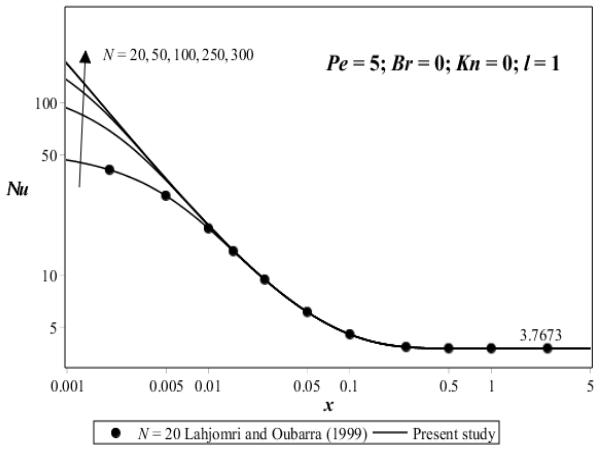


(a) $l = 1$

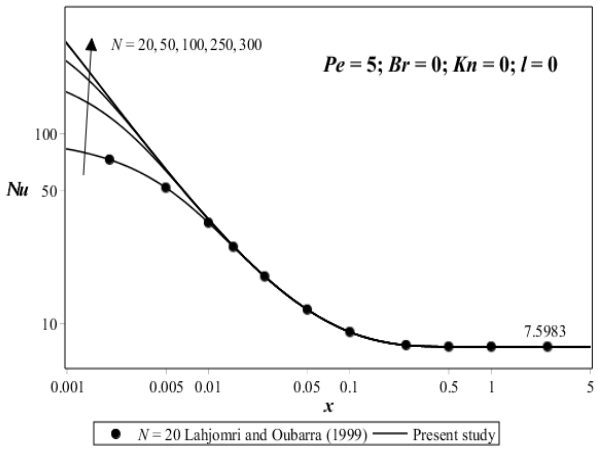


(b) $l = 0$

**Fig. 3** Evolution of the local Nusselt number as a function of $x$ for $N = 20, 50, 100, 250, 300$, $Pe = 5$, and $Br = 0$ as well as a comparison with the results of Lahjomri and Oubarra (1999) in: (a) a tube and (b) a channel.

For small Péclet numbers, the increase of the eigenvalues $\beta_n$ and the decrease of the expansion constants $B_n$ in the series become slower, which requires larger values of the truncation order to achieve accurate results near the junction point. Sphaier *et al.* (2021) presented an error analysis of the Nusselt number as a function of the truncation order for different values of the flow parameters. They concluded that the Nusselt error, as expected, decreases with the increase of the truncation order while it increases with the decrease of the Péclet number or near the junction point with few exceptions that occur near a discontinuity in the Nusselt number. They found that using similar types of boundary conditions, a fixed constant wall temperature or a fixed uniform heat flux in both regions, upstream and downstream, yields smaller Nusselt errors.

## 4. RESULTS AND DISCUSSIONS

The effects of axial heat conduction, viscous dissipation, and rarefaction on the extended Graetz problem in microchannels and microtubes with imposed average velocity are widely presented in the literature (Jeong and Jeong, 2006; Çetin *et al.*, 2008; Çetin and Zeinali, 2014; Barişik *et al.*, 2015; Kalyoncu and Barişik, 2016; Haddout *et al.*, 2020; Sun *et al.*, 2020). However, there is a lack of results in the case of imposed pressure drop. For the no-slip flow regime, the results are identical either the average velocity or the pressure drop is imposed. Therefore, the results presented in this section focus on the slip flow regime with imposed pressure drop as well as a comparison with the case of imposed average velocity. The effects of the Knudsen number and the degree of temperature jump are presented for negligible axial heat conduction and no viscous dissipation, as well as in the case including axial heat conduction and viscous dissipation. The Knudsen number is varied within the range of the applicability limits of the no-slip flow and the slip flow, $0 \leq Kn \leq 0.1$. The degrees of temperature jump used in this section are $\kappa = 0, 1.667, 5, 10$. The case $\kappa = 0$ is presented to investigate the effect of the slip-velocity with no-temperature-jump at the walls, $\kappa = 1.667$ is a typical value widely used in literature which represents the value for air that is a working fluid in many industrial and engineering applications (Çetin *et al.*, 2008), while $\kappa = 5, 10$ are included to exemplify the effects of the temperature jump at the walls. The pure diffuse reflection (Beskok and Kamiadakis, 1994), $\sigma_v = 1$, is considered in what follows. For $Kn = 0$, there is no-temperature-jump even with $\kappa \neq 0$ due to the appearance of $\kappa$ multiplied by $Kn$ in the temperature jump at the walls, as can be seen from Eqs. (16) and (17).

### 4.1 Slip Flow Regime Case

In this sub-section, the results for the local Nusselt number in a microtube or a microchannel are presented in the case of the slip flow, $Kn \neq 0$, for negligible axial heat conduction and no viscous dissipation with imposed pressure drop for different Knudsen numbers and degrees of temperature jump. In addition to that, these results are compared with the case of imposed average velocity.

Figures 4(a) and 4(b) show the evolution of $Nu$ as a function of $x$ for different Knudsen numbers $Kn = 0, 0.01, 0.05, 0.1$, no-viscous dissipation $Br = 0$, no-temperature-jump $\kappa = 0$, and negligible axial heat conduction $Pe = \infty$ with imposed pressure drop respectively in a microtube $(l = 1)$ and a microchannel $(l = 0)$. The results show that $Nu$ increases as $Kn$ increases similarly for $Nu_{FD}$ in both microchannels and microtubes. This is due to the slip-velocity at the walls that increases as the Knudsen number increases, which leads to higher heat transfer. The length of the thermal entrance increases as well with the increase of $Kn$ due to the slip-velocity at the walls, which induces an increase in the convective term in the energy equation, Eq. (15), and therefore leads to a more dominant convective heat transfer to conduction heat transfer in the thermal entrance region.

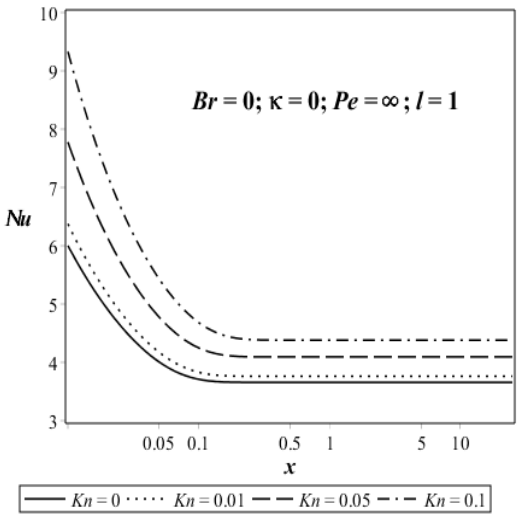


(a) $l = 1$

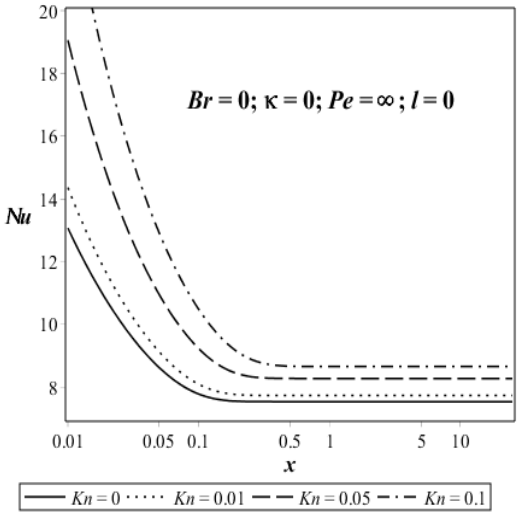


(b) $l = 0$

**Fig. 4** Evolution of $Nu$ as a function of $x$ for $Kn = 0, 0.01, 0.05, 0.1$, $Br = 0$, $Pe = \infty$ and $\kappa = 0$ with imposed pressure drop in: (a) a microtube and (b) a microchannel.

As shown in Figs. 4(a) and 4(b), the results are qualitatively similar for a microtube and a microchannel with quantitative differences. At section $x = 0.05$, $Nu$ increases by 35.5% when $Kn$ changes from 0 to 0.1 in the microtube ($l = 1$) and by 49.7% in the microchannel ($l = 0$) for the same values. Therefore, what follows in this section focuses only on the microtube case ($l = 1$).

To obtain the temperature profile for the case of fixed average velocity, the Péclet number, Brinkman number, dimensionless longitudinal coordinate, and the dimensionless velocity distribution must be redefined in terms of the average velocity. Thus, the modified versions of $Pe$, $Br$, $x$, and $u$ are defined as follows:

$$x = X\frac{l+3}{2}\left(\frac{2}{l+3} + 2^{3-l}\frac{2-\sigma_v}{\sigma_v}Kn\right);\quad u(\eta) = U(\eta)\left(\frac{2}{l+3} + 2^{3-l}\frac{2-\sigma_v}{\sigma_v}Kn\right);$$
$$Pe = \frac{Pe_U}{\frac{l+3}{2}\left(\frac{2}{l+3}+2^{3-l}\frac{2-\sigma_v}{\sigma_v}Kn\right)};\quad Br = \frac{Br_U}{\left(\frac{2}{l+3}+2^{3-l}\frac{2-\sigma_v}{\sigma_v}Kn\right)^2} \qquad (61)$$

where $Pe_U = \frac{l+3}{2}\frac{\rho C_p d U_{ave}}{k}$, $Br_U = \frac{\mu {U_{ave}}^2}{k(T_{w1}-T_{w2})}$, $X = \frac{x^*}{d\,Pe_U}$, and $U = \frac{u^*}{U_{ave}}$ are respectively the new defined Péclet number, Brinkman number, dimensionless longitudinal coordinate, and the dimensionless velocity distribution in terms of the average velocity. The proportionality in Eq. (61) is obtained using Eq. (60) to change $\Delta p_L^*$ in terms of $U_{ave}$. Equation (61) for $Kn = 0$ leads to $Pe = Pe_U$ and $x = X$.

To compare the results in the case of imposed pressure drop with the results in the case of imposed average velocity, unified dimensionless variables and numbers must be defined in terms of a reference pressure drop $\Delta p_{L_0}^*$ and a reference average velocity $U_{ave_0}$ that are related by Eq. (60) for $Kn = 0$. In the case of imposed pressure drop, $\Delta p_L^* = \Delta p_{L_0}^*$ and $U_{ave}$ is determined for different Knudsen numbers by using Eq. (60), while in the case of imposed average velocity, $U_{ave} = U_{ave_0}$ and $\Delta p_L^*$ is determined for different Knudsen numbers by using Eq. (60). The reference dimensionless longitudinal coordinate, the Péclet number and Brinkman number are defined in terms of $\Delta p_{L_0}^*$ and $U_{ave_0}$ as follows:

$$x_0 = \frac{x^*}{d\,Pe_0};\quad Pe_0 = \frac{\rho C_p d^3}{2(l+1)\mu k}\Delta p_{L_0}^* = \frac{l+3}{2}\frac{\rho C_p d}{k}U_{ave_0};$$
$$Br_0 = \frac{d^4}{4(l+1)^2\mu k(T_{w1}-T_{w2})}\left(\Delta p_{L_0}^*\right)^2 = \left(\frac{l+3}{2}\right)^2\frac{\mu}{k(T_{w1}-T_{w2})}{U_{ave_0}}^2 \qquad (62)$$

In the case of a no-slip flow regime, the results for the fixed pressure drop are identical to those for the fixed average velocity due to the proportionality between $\Delta p_{L_0}^*$ and $U_{ave_0}$. In contrast, in the case of the slip flow regime, the results are no longer identical due to the change in $U_{ave}$ with $Kn$ for fixed pressure drop, Eq. (60). To use the analytical solution presented in section 2, $Pe_0$, $Br_0$, and $x_0$ must be defined in terms of $Pe$, $Br$, and $x$ for each case (a fixed $\Delta p_L^*$ and a fixed $U_{ave}$).

For a fixed pressure drop $\left(\Delta p_L^* = \Delta p_{L_0}^*\right)$, the following relationships are obtained:

$$Pe_0 = Pe;\quad Br_0 = Br;\quad x_0 = x \qquad (63)$$

where $U_{ave}$ is determined using Eq. (60).

For a fixed average velocity $\left(U_{ave} = U_{ave_0}\right)$, the following relationships are obtained:

$$Pe_0 = Pe_U = \frac{l+3}{2}\left(\frac{2}{l+3} + 2^{3-l}\frac{2-\sigma_v}{\sigma_v}Kn\right)Pe;\quad Br_0 = \left(\frac{l+3}{2}\right)^2 Br_U =$$
$$\left(\frac{l+3}{2}\right)^2\left(\frac{2}{l+3} + 2^{3-l}\frac{2-\sigma_v}{\sigma_v}Kn\right)^2 Br;\quad x_0 = X = \frac{x}{\frac{l+3}{2}\left(\frac{2}{l+3}+2^{3-l}\frac{2-\sigma_v}{\sigma_v}Kn\right)} \qquad (64)$$

where the proportionalities in Eq. (64) are obtained using Eq. (61).

Figure 5 shows a comparison between the evolution of $Nu$ as a function of $x_0 = \frac{x^*}{d \cdot Pe_0}$ for different Knudsen numbers $Kn = 0, 0.05, 0.1$ in a microtube ($l = 1$) with no-temperature-jump at the walls ($\kappa = 0$), no viscous dissipation ($Br_0 = 0$), and negligible axial heat conduction ($Pe_0 = \infty$) in both cases of fixed pressure drop and fixed average velocity. The results show that $Nu$ in the developing region is larger for the case of imposed pressure drop compared to the case of imposed average velocity, and the thermal entrance length increases as well. This is due to the increase of the average velocity with the increase of the Knudsen number in the case of imposed pressure drop $\left(\Delta p_L^* = \Delta p_{L_0}^*\right)$ as opposed to the case of imposed average velocity where it is fixed as $U_{ave} = U_{ave_0}$.

Note that the loss in the thermal performance for a fixed average velocity is gained in the pressure drop along the streamwise direction per unit length, which decreases as Knudsen number increases $\left(\Delta p_L^* = \frac{2(l+1)\mu}{d^2}\cdot\frac{U_{ave_0}}{\left(\frac{2}{l+3}+2^{3-l}\frac{2-\sigma_v}{\sigma_v}Kn\right)}\right)$. $Nu$ for a fixed average velocity increases as $Kn$ increases because of slip-velocity at the walls. At section $x_0 = 0.05$, $Nu$ increases by 35.5% when $Kn$ changes from 0 to 0.1 for an imposed pressure drop and by 19% for an imposed average velocity with the same values. $Nu_{FD}$ is the same in both cases of imposed pressure drop and imposed average velocity for the different Knudsen numbers

Global Digital Central
ISSN: 2151-8629

due to the fact that at $x_0 = +\infty$, the convective term in the energy equation does not affect the results anymore $\left(\left.\frac{\partial T_2}{\partial x_0}\right|_{x_0=+\infty} = 0\right)$.

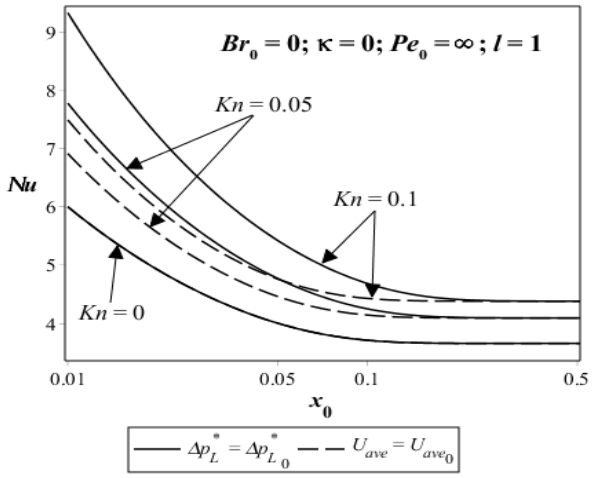


**Fig. 5** Evolution of $Nu$ as a function of $x_0$ for different Knudsen numbers in a microtube with $\kappa = 0$, $Br_0 = 0$, and $Pe_0 = \infty$ in both cases of a fixed $\Delta p_L^*$ and a fixed $U_{ave}$.

The solution to the presented problem is unique. However using different characteristic parameters lead to different presentations of the results where one gives a different idea and can have a significant impact, especially for optimization problems.

In addition to the slip-velocity at the walls, the temperature jump also plays a significant role in heat transfer. Figure 6 shows the evolution of $Nu$ as a function of $x$ for different degrees of temperature jump $\kappa = 0, 1.667, 5, 10$, $Kn = 0.1$, no-viscous dissipation $Br = 0$, and negligible axial heat conduction $Pe = \infty$ with imposed pressure drop in a microtube ($l = 1$). The results show that $Nu$ and $Nu_{FD}$ decrease significantly as the degree of temperature jump, $\kappa$, increases. This is due to the increase of the temperature jump at the walls, Eq. (17), which increases the dimensionless bulk temperature. The presence of the temperature jump also reduces heat conduction at the walls (Çetin and Zeinali, 2014).

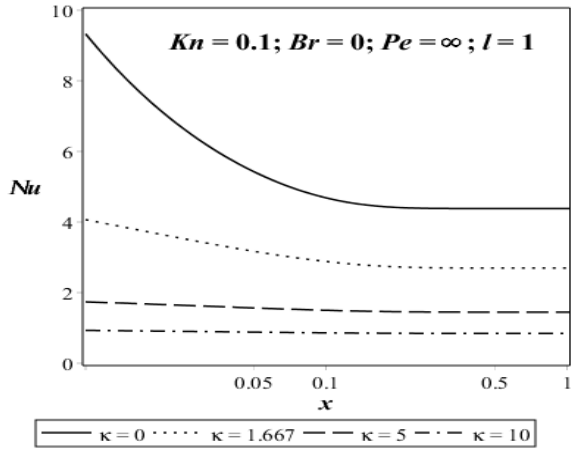


**Fig. 6** Evolution of $Nu$ as a function of $x$ for different degrees of temperature jump, $Kn = 0.1$, $Pe = \infty$, and $Br = 0$ with imposed pressure drop in a microtube.

To compare the results with and without the temperature jump at the walls in the case of a fixed pressure drop with those of a fixed average velocity, the unified dimensionless variables and numbers are introduced by using Eqs. (63) and (64) respectively for $\Delta p_L^* = \Delta p_{L_0}^*$ and $U_{ave} = U_{ave_0}$. Figures 7(a) and 7(b) show respectively the evolution of $Nu$ (at section $x_0 = 0.05$) and $Nu_{ave} = \frac{1}{0.21}\int_0^{0.21} Nu(x_0)dx_0$ as a function of $Kn$ in a microtube with and without the temperature jump at the walls ($\kappa = 0, 1.667$), no viscous dissipation ($Br_0 = 0$), and negligible axial heat conduction ($Pe_0 = \infty$) for a fixed pressure drop and a fixed average velocity. To obtain the value of the average Nusselt number $Nu_{ave}$, the local Nusselt number is averaged from the junction point ($x_0 = 0$) to the largest thermal entrance length ($x_0 = 0.21$), which is the length required to achieve 101% of the fully developed Nusselt number, for the values presented in Fig. 7(b). The results show that $Nu$ increases with increasing $Kn$ in the case of no-temperature-jump condition at the walls while it decreases with increasing $Kn$ in the case of the temperature jump at the walls. The same conclusions derived from Fig. 5 are observed in Figs. 7(a) and 7(b), which represent respectively one section ($x_0 = 0.05$) and the average over the largest thermal entrance length. At section $x_0 = 0.05$ for $Kn = 0.1$ and $\kappa = 1.667$, $Nu$ increases by 8.6% when the results change from imposed average velocity to imposed pressure drop with the same values. Fig. 7(b) shows that for $Kn = 0.1$, $Nu_{ave}$ increases by 10.3% when the results change from imposed average velocity to imposed pressure drop for $\kappa = 0$ and by 5.3% for $\kappa = 1.667$ with the same values.

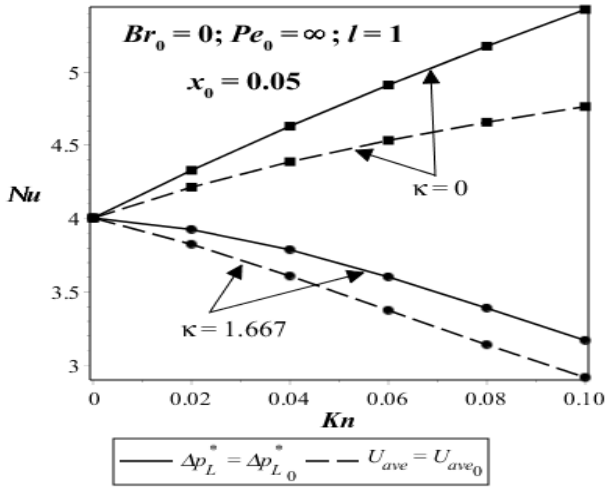


(a) $Nu$ ($x_0 = 0.05$)

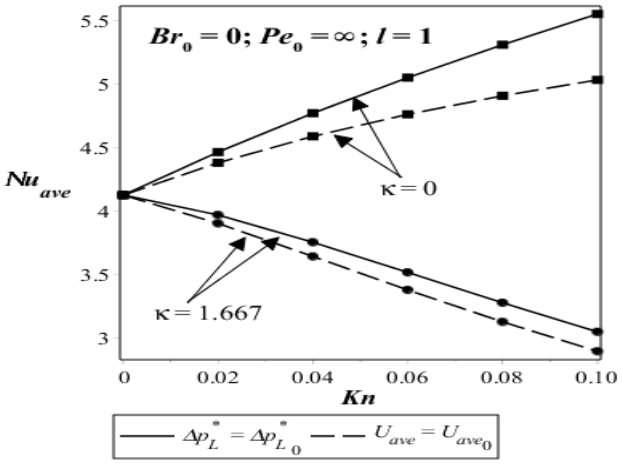


(b) $Nu_{ave}$

**Fig. 7** Evolution of $Nu$ (at section $x_0 = 0.05$) and $Nu_{ave}$ (between $x_0 = 0$ and 0.21) as a function of $Kn$ in a microtube with $\kappa = 0, 1.667$, $Br_0 = 0$, and $Pe_0 = \infty$ for a fixed $\Delta p_L^*$ and a fixed $U_{ave}$.

Global Digital Central
ISSN: 2151-8629

The thermal entrance length is defined as the length required to reach the fully developed region by approximately achieving the value of the fully developed Nusselt number with different reported criteria, somewhat arbitrary, used in the literature (Shah and London, 1978). To compare the thermal entrance lengths for different Knudsen numbers and degrees of temperature jump in this paper, the length required to achieve $Nu = 1.01 \cdot Nu_{FD}$ is considered as the thermal entrance length. Table 3 shows the thermal entrance length in the case of an imposed pressure drop $\left(\Delta p_L^* = \Delta p_{L_0}^*\right)$ and an imposed average velocity $\left(U_{ave} = U_{ave_0}\right)$ in a microtube $(l = 1)$ for $Kn = 0, 0.02, 0.04, 0.06, 0.08, 0.1$, $\kappa = 0, 1.667$, $Br_0 = 0$, and $Pe_0 = \infty$. As can be seen from Table 3, the thermal entrance length increases as $Kn$ or $\kappa$ increases in the case of imposed pressure drop, which can be observed in Figs. 4(a) and 6. However, in the case of imposed average velocity with no viscous dissipation and negligible axial heat conduction, it is found that the thermal entrance length is slightly modified when increasing Knudsen numbers and degrees of temperature jump (~0.11). Table 3 shows that approximately there is a proportionality between the thermal entrance length in the case of fixed pressure drop and the case of fixed average velocity, which is similar to the proportionality between $x$ and $X$ (Eq. (61)).

**Table 3** The thermal entrance length in the case of an imposed pressure drop and an imposed average velocity in a microtube for different Knudsen numbers and degrees of temperature jump with negligible axial heat conduction and no viscous dissipation.

| $\kappa$ | $Kn$ | Thermal entrance length | | $Nu_{FD}$ |
|---|---|---|---|---|
| | | $\Delta p_L^* = \Delta p_{L_0}^*$ | $U_{ave} = U_{ave_0}$ | |
| 0 | 0 | 0.1101 | 0.1101 | 3.65679 |
| | 0.02 | 0.1247 | 0.1075 | 3.85558 |
| | 0.04 | 0.1393 | 0.1055 | 4.02067 |
| | 0.06 | 0.1538 | 0.1040 | 4.15989 |
| | 0.08 | 0.1684 | 0.1027 | 4.27885 |
| | 0.1 | 0.1828 | 0.1016 | 4.38166 |
| 1.667 | 0.02 | 0.1305 | 0.1125 | 3.48809 |
| | 0.04 | 0.1516 | 0.1148 | 3.29166 |
| | 0.06 | 0.1723 | 0.1164 | 3.08705 |
| | 0.08 | 0.1919 | 0.1170 | 2.88646 |
| | 0.1 | 0.2100 | 0.1167 | 2.69667 |
| 5 | 0.02 | 0.1358 | 0.1171 | 2.90180 |
| | 0.04 | 0.1539 | 0.1166 | 2.35607 |
| | 0.06 | 0.1665 | 0.1125 | 1.96130 |
| | 0.08 | 0.1755 | 0.1070 | 1.66958 |
| | 0.1 | 0.1824 | 0.1014 | 1.44822 |

## 4.2 Slip Flow Regime Case with Axial Heat Conduction and Viscous Dissipation

In this sub-section, the effects of the slip flow coupled with the axial heat conduction and viscous dissipation are investigated for a microtube $(l = 1)$ with a comparison between the cases of imposed pressure drop and imposed average velocity. To obtain the average Nusselt number $Nu_{ave}$ in this case, the local Nusselt number is averaged from the junction point $(x_0 = 0)$ to the largest thermal entrance length $(x_0 = 2.07)$ and $Nu_{ave} = \frac{1}{2.07}\int_0^{2.07} Nu(x_0)dx_0$.

Figures 8(a)-(c) show respectively the evolution of $Nu$ as a function of $x_0$ for $Kn = 0.1$, $\kappa = 0$, $Br_0 = 0.1$, and $Pe_0 = \infty$, $Nu_{ave}$ as a function of $Kn$ for $\kappa = 0, 1.667$, $Br_0 = 0.1$, and $Pe_0 = 5, \infty$ in a microtube with both cases of a fixed pressure drop $\left(\Delta p_L^* = \Delta p_{L_0}^*\right)$ and a fixed average velocity $\left(U_{ave} = U_{ave_0}\right)$. It is found that $Nu_{ave}$ does not change much with viscous dissipation. However, for $Nu$ with viscous dissipation, there is a difference in behavior between the cases of imposed pressure drop and imposed average velocity. The results show that the quantitative differences in $Nu_{ave}$ between the case of imposed pressure drop and imposed average velocity are reduced with axial heat conduction (small $Pe_0$) and viscous dissipation (large $Br_0$) effects.

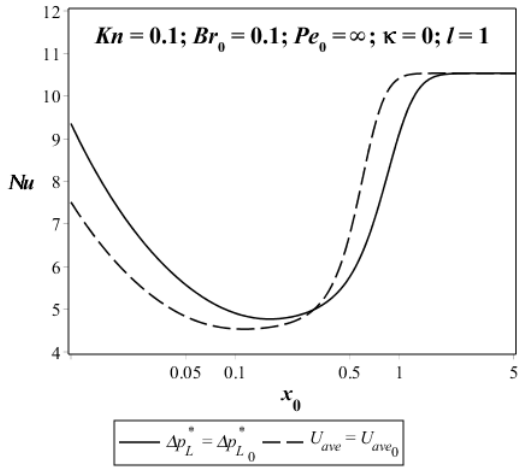


(a) $Nu(x_0)$ with $Pe_0 = \infty$

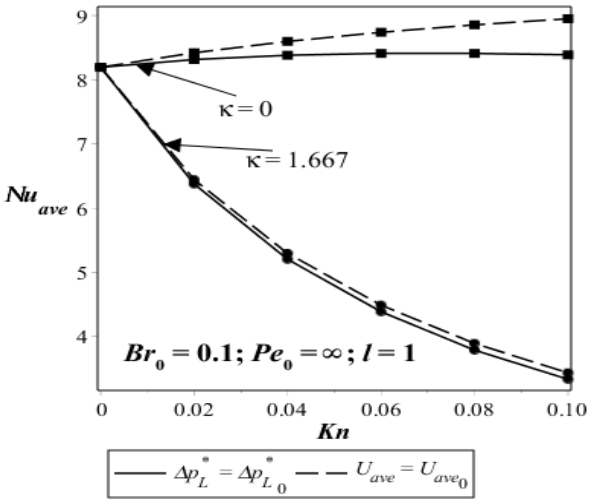


(b) $Nu_{ave}(Kn)$ with $Pe_0 = \infty$

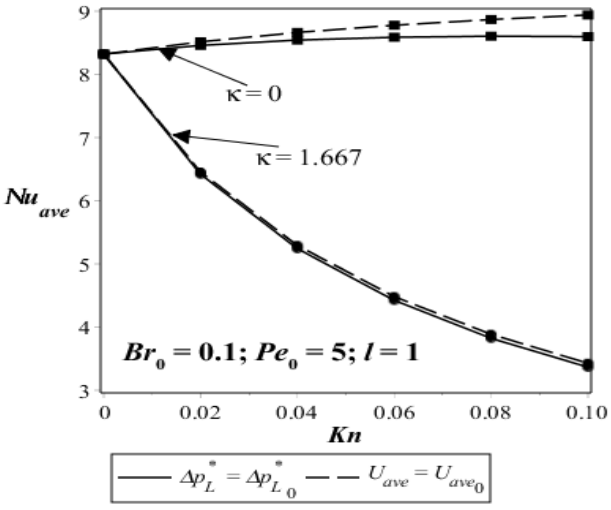


(c) $Nu_{ave}(Kn)$ with $Pe_0 = 5$

**Fig. 8** Evolution of $Nu$ as a function of $x_0$ $(Kn = 0.1, \kappa = 0, Pe_0 = \infty)$ and $Nu_{ave}$ as a function of $Kn$ $(\kappa = 0, 1.667, Pe_0 = 5, \infty)$ in a microtube with $Br_0 = 0.1$ for a fixed $\Delta p_L^*$ and a fixed $U_{ave}$.

Global Digital Central
ISSN: 2151-8629

Let us note that for $Br \neq 0$, to obtain the fully developed Nusselt number expressions, the dimensionless temperature profile, Eq. (24), and its derivative are used to calculate the dimensionless bulk temperature, Eq. (59), and the fully developed Nusselt number using Eq. (58). The fully developed Nusselt number for $Br \neq 0$ respectively in a microtube ($l = 1$) and a microchannel ($l = 0$) is given by:

$$Nu_{FD} = \frac{48\left(1+8\frac{2-\sigma_v}{\sigma_v}Kn\right)}{5+32\frac{2-\sigma_v}{\sigma_v}Kn+48\kappa Kn+384\frac{2-\sigma_v}{\sigma_v}\kappa Kn^2} \quad (65)$$

$$Nu_{FD} = \frac{35\left(1+12\frac{2-\sigma_v}{\sigma_v}Kn\right)}{2+21\frac{2-\sigma_v}{\sigma_v}Kn+35\kappa Kn+420\frac{2-\sigma_v}{\sigma_v}\kappa Kn^2} \quad (66)$$

Equations (65) and (66) show that $Nu_{FD}$ is independent of the Péclet number and the Brinkman number in the presence of viscous dissipation. These results, after rearrangements, are found to be identical to those presented by Jeong and Jeong (2006) for an imposed average velocity due to their independence of the parameters that differ depending on the case studied (imposed $\Delta p_L^*$ or imposed $U_{ave}$). It can be verified using Eqs. (65) and (66) that the fully developed Nusselt number with viscous dissipation increases with increasing Knudsen numbers for no-temperature-jump condition. In the case of the temperature jump at the walls, the fully developed Nusselt number decreases with the increase of the Knudsen number or the degree of temperature jump.

## 5. CONCLUSIONS

An exact analytical solution of the extended Graetz problem in microchannels and microtubes with axial heat conduction, viscous dissipation, and rarefaction effects was presented using constant wall temperatures and taking into account the slip-velocity and the temperature jump at the walls using first-order models as well as the non-uniform temperature profile at the inlet of the microchannel or microtube for the case of imposed pressure drop along the streamwise direction per unit length. The dimensionless temperature distribution is written as a superposition of the dimensionless fully developed temperature and an expansion in terms of a complete set that leads to an eigenvalue problem where the eigenfunctions are given by Kummer confluent first-kind hypergeometric functions. The eigenvalues are determined as roots of equations derived from the boundary conditions, while the expansion constants are calculated using direct expressions. To the best of our knowledge, this case of imposed pressure drop along the streamwise direction per unit length has still not been investigated. The analytical solution for a fixed average velocity can be obtained using the presented solution in this paper by redefining the Péclet number, Brinkman number, dimensionless longitudinal coordinate, and the dimensionless velocity distribution. However, the proposed methodology in this paper has an advantage over the analytical procedure in the literature due to the direct resolution without introducing the spatial rescaling factor, which is needed for the case of fixed average velocity to identify similarities with the classical Graetz problem. The presented solution of the laminar forced convection in parallel plate microchannels and circular microtubes for the case of imposed pressure drop can be the reference solution for shape optimization problems to enhance heat transfer while using a fixed pressure drop.

The following main conclusions can be summarized:

- The Nusselt number increases with the increase of the Knudsen number in the case of no-temperature-jump condition at the walls.
- In the case of the temperature jump at the walls, the Nusselt number decreases as the Knudsen number or the degree of temperature jump increases.
- The thermal entrance length increases with the increase of the Knudsen number or the degree of the temperature jump in the case of imposed pressure drop while it is approximately unchangeable in the case of imposed average velocity.
- For no viscous dissipation and negligible axial heat conduction, the local Nusselt number is larger for imposed pressure drop compared to imposed average velocity.
- There is a difference in the behavior of the local Nusselt number with viscous dissipation between the cases of imposed pressure drop and imposed average velocity.
- The quantitative differences between the cases of imposed pressure drop and imposed average velocity in the average Nusselt number over the largest thermal entrance length are reduced with increasing axial heat conduction or viscous dissipation effects.
- The fully developed Nusselt number is the same for imposed pressure drop and imposed average velocity.

## ACKNOWLEDGEMENTS

This work is done with the financial support of the National Center for Scientific and Technical Research (CNRST).

## NOMENCLATURE

| | |
|---|---|
| *A, B* | expansion constants |
| *a, b, c* | coefficients of Kummer function |
| *Br* | Brinkman number |
| $C_p$ | specific heat (J/kg·K) |
| $D_h$ | hydraulic diameter (m) |
| *d* | half height or radius (m) |
| *f, g* | eigenfunctions |
| *Kn* | Knudsen number |
| *k* | thermal conductivity (W/m·K) |
| *l* | geometrical parameter |
| *M* | Kummer function |
| *N* | truncation order |
| *Nu* | Nusselt number |
| *Pe* | Péclet number |
| *Pr* | Prandtl number |
| *p* | pressure |
| *q* | heat flux (W/m$^2$) |
| *T* | temperature |
| *u* | axial velocity |
| *x* | longitudinal coordinate |

*Greek Symbols*

| | |
|---|---|
| *α, β* | eigenvalues |
| *γ* | specific heat ratio |
| *η* | transversal or radial coordinate |
| *κ* | degree of temperature jump |
| *λ* | mean free path (m) |
| *μ* | dynamic viscosity (kg/m·s) |
| *ρ* | density (kg/m$^3$) |
| *σ* | accommodation coefficient |

*Superscripts*

| | |
|---|---|
| * | dimensional |

*Subscripts*

| | |
|---|---|
| *1* | upstream ($x < 0$) |
| *2* | downstream ($x > 0$) |
| *ave* | average |
| *b* | bulk |
| *FD* | fully developed |
| *j* | upstream or downstream |
| *n, m* | summation indexes |
| *w* | wall |

## REFERENCES

Al-Gburi, H., Mohammed, A.A., and Al-Abbas, A.H., 2023, "Experimental study of the thermal performance of corrugated helically coiled tube-in-tube heat exchanger," *Front. Heat Mass Transf.*, **20**, 17. https://doi.org/10.5098/hmt.20.17

Barişik, M., Yazicioğlu, A.G., Çetin, B., and Kakaç, S., 2015, "Analytical solution of thermally developing microtube heat transfer including axial conduction, viscous dissipation, and rarefaction effects," *Int. Commun. Heat Mass Transfer*, **67**, 81-88. https://doi.org/10.1016/j.icheatmasstransfer.2015.05.004

Beskok, A., and Karniadakis, G.E., 1994, "Simulation of heat and momentum transfer in complex microgeometries," *J. Thermophys. Heat Trans.*, **8**(4), 355-370. https://doi.org/10.2514/3.594

Çetin, B., Yazicioğlu, A.G., and Kakaç, S., 2008, "Fluid flow in microtubes with axial conduction including rarefaction and viscous dissipation," *Int. Commun. Heat Mass Transfer*, **35**(5), 535-544. https://doi.org/10.1016/j.icheatmasstransfer.2008.01.003

Çetin, B., and Zeinali, S., 2014, "Analysis of heat transfer and entropy generation for a low-Peclet-number microtube flow using a second-order slip model: an extended-Graetz problem," *J. Eng. Math.*, **89**, 13-25. https://doi.org/10.1007/s10665-014-9704-7

Chung, J.N., Chen, T., and Maroo, S.C., 2011, "A review of recent progress on nano/micro scale nucleate boiling fundamentals," *Front. Heat Mass Transf.*, **2**, 023004. https://doi.org/10.5098/hmt.v2.2.3004

Dutta, P., Horiuchi, K., and Yin, H.M., 2006, "Thermal characteristics of mixed electroosmotic and pressure-driven microflows," *Comput. Math. Appl.*, **52**(5), 651-670. https://doi.org/10.1016/j.camwa.2006.10.002

Fabbri, G., 2000, "Heat transfer optimization in corrugated wall channels," *Int. J. Heat Mass Transfer*, **43**(23), 4299-4310. https://doi.org/10.1016/S0017-9310(00)00054-5

Gad-el-Hak, M., 1999, "The fluid mechanics of microdevices – the Freeman scholar lecture," *J. Fluids Eng.*, **121**(1), 5-33. https://doi.org/10.1115/1.2822013

Gao, J., Hu, Z., Yang, Q., Liang, X., and Wu, H., 2022, "Fluid flow and heat transfer in microchannel heat sinks: Modeling review and recent progress," *Therm. Sci. Eng. Prog.*, **29**, 101203. https://doi.org/10.1016/j.tsep.2022.101203

Graetz, L., 1882, "Ueber die wärmeleitungsfähigleit von flüssigkeiten," *Ann. Phys.*, **254**(1), 79-94. https://doi.org/10.1002/andp.18822540106

Gulia, V., and Sur, A., 2022, "A comprehensive review on microchannel heat exchangers, heat sink, and polymer heat exchangers: Current state of the art," *Front. Heat Mass Transf.*, **18**, 40. https://doi.org/10.5098/hmt.18.40

Haddout, Y., Oubarra, A., and Lahjomri, J., 2020, "Heat transfer in the slip flow with axial heat conduction in a microchannel with walls having a constant temperature," *J. Eng. Phys. Thermophys.*, **93**, 625-636. https://doi.org/10.1007/s10891-020-02158-9

Han, Y., Liu, Y., Li, M., and Huang, J., 2012, "A review of development of micro-channel heat exchanger applied in air-conditioning system," *Energy Procedia*, **14**, 148-153. https://doi.org/10.1016/j.egypro.2011.12.910

Hennecke, D.K., 1968, "Heat transfer by Hagen-Poiseuille flow in the thermal development region with axial conduction," *Wärme- und Stoffübertragung*, **1**, 177-184. https://doi.org/10.1007/BF00751149

Ismail, M.F., Rashid, M.A.I, and Mahbub, M., 2012, "Numerical simulation of fluid flow and heat transfer in a MEMS-based micro channel heat sink," *Front. Heat Mass Transf.*, **3**, 033002. https://doi.org/10.5098/hmt.v3.3.3002

Jaddoa, A.A., Hamad, K.A., and Hameed, A.A.J., 2023, "Fluid inflow and heat transfer enhancement: An experimental analysis of nanofluids in mini-channel," *Front. Heat Mass Transf.*, **20**, 18. https://doi.org/10.5098/hmt.20.18

Jeong, H., and Jeong, J., 2006, "Extended Graetz problem including streamwise conduction and viscous dissipation in microchannel," *Int. J. Heat Mass Transfer*, **49**(13-14), 2151-2157. https://doi.org/10.1016/j.ijheatmasstransfer.2005.11.026

Jeong, H., and Jeong, J., 2006, "Extended Graetz problem including axial conduction and viscous dissipation in microtube," *J. Mech. Sci. Technol.*, **20**(1), 158-166. https://doi.org/10.1007/BF02916209

Kalyoncu, G., and Barişik, M., 2016, "The extended Graetz problem for micro-slit geometries; analytical coupling of rarefaction, axial conduction and viscous dissipation," *Int. J. Therm. Sci.*, **110**, 261-269. https://doi.org/10.1016/j.ijthermalsci.2016.07.009

Kanor, A., and Manimaran, R., 2016, "Effect of different shapes on characteristics of conjugate heat transfer of micro channel heat sink," *Front. Heat Mass Transf.*, **7**, 25. https://doi.org/10.5098/hmt.7.25

Khan, M.G., and Fartaj, A., 2011, "A review on microchannel heat exchangers and potential applications," *Int. J. Energy Res.*, **35**(7), 553-582. https://doi.org/10.1002/er.1720

Khatyr, R., and Khalid Naciri, J., 2022, "Effects of viscous dissipation and axial heat conduction on forced convection duct flow of Herschel-Bulkley fluid with uniform wall temperature or convective boundary conditions," *Front. Heat Mass Transf.*, **19**, 23. https://doi.org/10.5098/hmt.19.23

Lahjomri, J., and Oubarra, A., 1999, "Analytical solution of the Graetz problem with axial conduction," *J. Heat Transfer*, **121**(4), 1078-1083. https://doi.org/10.1115/1.2826060

Larrodé, F.E., Housiadas, C., and Drossinos, Y., 2000, "Slip-flow heat transfer in circular tubes," *Int. J. Heat Mass Transfer*, **43**(15), 2669-2680. https://doi.org/10.1016/S0017-9310(99)00324-5

Papoutsakis, E., Damkrishna, D., and Lim, H.C., 1980, "The extended Graetz problem with Dirichlet wall boundary conditions," *Appl. Sci. Res.*, **36**, 13-34. https://doi.org/10.1007/BF00420067

Qasem, N.A.A., and Zubair, S.M., 2018, "Compact and microchannel heat exchangers: A comprehensive review of air-side friction factor and heat transfer correlations," *Energy Convers. Manag.*, **173**, 555-601. https://doi.org/10.1016/j.enconman.2018.06.104

Ramesh, K.N., Sharma, T.K., and Rao, G.A.P., 2021, "Latest advancements in heat transfer enhancement in micro-channel heat sinks: A review," *Arch. Comput. Methods Eng.*, **28**, 3135-3165. https://doi.org/10.1007/s11831-020-09495-1

Rosa, P., Karayiannis, T.G., and Collins, M.W., 2009, "Single-phase heat transfer in microchannels: The importance of scaling effects," *Appl. Therm. Eng.*, **29**(17-18), 3447-3468.

https://doi.org/10.1016/j.applthermaleng.2009.05.015

Shah, R.K., and London, A.L., 1978, *Laminar flow forced convection in ducts*, 1st ed., Academic Press, New York.

Soheel, A.H., Jumaah, O.M., and Saleem, A.M., 2021, "Simulation and investigation of nano-refrigerant fluid characteristics with two-phase flow in microchannel," *Front. Heat Mass Transf.*, **17**, 21.
https://doi.org/10.5098/hmt.17.21

Sparrow, E.M., and Lin, S.H., 1962, "Laminar heat transfer in tubes under slip-flow conditions," *J. Heat Transfer*, **84**(4), 363-369.
https://doi.org/10.1115/1.3684399

Sphaier, L.A., Braga Jr., N.R., and Chalhub, D.J.N.M., 2021, "Analytical solutions for extended Graetz problem in infinite domains via integral transforms," *Int. J. Therm. Sci.*, **170**, 107093.
https://doi.org/10.1016/j.ijthermalsci.2021.107093

Sun, Q., Choi, K., and Mao, X., 2020, "An analytical solution of convective heat transfer in microchannel or nanochannel," *Int. Commun. Heat Mass Transfer*, **117**, 104766.
https://doi.org/10.1016/j.icheatmasstransfer.2020.104766

Tian, Y., Long, C., and Tang, L., 2022, "Study on thermal-hydraulic performance of the printed circuit heat exchanger with airfoil fins for supercritical liquefied natural gas," *Front. Heat Mass Transf.*, **19**, 18.
https://doi.org/10.5098/hmt.19.18

Turkyilmazoglu, M., 2021a, "Heat transport in shear-driven flow with axial conduction," *J. Taiwan Inst. Chem. Eng.*, **123**, 96-103.
https://doi.org/10.1016/j.jtice.2021.05.038

Turkyilmazoglu, M., 2021b, "Heat absorption due to falling film with imposed uniform mass fraction at the wall," *Int. J. Heat Mass Transfer*, **177**, 121585.
https://doi.org/10.1016/j.ijheatmasstransfer.2021.121585

Turkyilmazoglu, M., 2022, "Thermal performance of optimum exponential fin profiles subjected to a temperature jump," *Int. J. Numer. Methods Heat Fluid Flow*, **32**(3), 1002-1011.
https://doi.org/10.1108/HFF-02-2021-0132

Tunc, G., and Bayazitoglu, Y., 2001, "Heat transfer in microtubes with viscous dissipation," *Int. J. Heat Mass Transfer*, **44**(13), 2395-2403.
https://doi.org/10.1016/S0017-9310(00)00298-2

Xu, B., Ooi, K.T., Mavriplis, C., and Zaghloul, M.E., 2003, "Evaluation of viscous dissipation in liquid flow in microchannels," *J. Micromech. Microeng.*, **13**(1), 53-57.
https://doi.org/10.1088/0960-1317/13/1/308

Zarita, R., and Hachemi, M., 2019, "Numerical investigation and analysis of heat transfer enhancement in a microchannel using nanofluids by the Lattice Boltzmann Method," *Front. Heat Mass Transf.*, **12**, 5.
https://doi.org/10.5098/hmt.12.5

Zhang, Y., 2017, "Modeling of micro/nano channel flows," *Front. Heat Mass Transf.*, **8**, 19.
https://doi.org/10.5098/hmt.8.19

## APPENDIX A: FULLY DEVELOPED TEMPERATURE PROFILES

$T_{-\infty}(\eta)$ and $T_{+\infty}(\eta)$ satisfy the governing equation, Eq. (15), and respectively the boundary conditions at the walls of the microchannel or microtube, Eqs. (16) and (17), hence the energy equation becomes:

$$0 = \frac{1}{\eta^l}\frac{d}{d\eta}\left(\eta^l \frac{dT_{\mp\infty}}{d\eta}\right) + Br\left(\frac{du}{d\eta}\right)^2 \tag{A.1}$$

with the following boundary conditions:

$$T_{-\infty}(\eta = 1) = 1 - 2^{2-l}\,\kappa\, Kn \left.\frac{dT_{-\infty}}{d\eta}\right|_{\eta=1} \tag{A.2}$$

$$T_{+\infty}(\eta = 1) = -2^{2-l}\,\kappa\, Kn \left.\frac{dT_{+\infty}}{d\eta}\right|_{\eta=1} \tag{A.3}$$

$$\left.\frac{dT_{\mp\infty}}{d\eta}\right|_{\eta=0} = 0 \tag{A.4}$$

Integrating Eq. (A.1) and using the boundary conditions, Eqs. (A.2)-(A.4), lead to the following solutions:

$$T_{-\infty}(\eta) = 1 + \frac{Br}{3+l}(1 - \eta^4 + 2^{4-l}\,\kappa\, Kn) \tag{A.5}$$

$$T_{+\infty}(\eta) = \frac{Br}{3+l}(1 - \eta^4 + 2^{4-l}\,\kappa\, Kn) \tag{A.6}$$

As can be seen from Eqs. (A.5) and (A.6), the relationship between the dimensionless temperature profiles $T_{-\infty}(\eta)$ and $T_{+\infty}(\eta)$ can be written as follows:

$$T_{-\infty}(\eta) = 1 + T_{+\infty}(\eta) \tag{A.7}$$

## APPENDIX B: FIRST 10 EXPANSION CONSTANTS

Table B.1 shows the first 10 expansion constants found by using Eqs. (54)-(57) for $Pe = 1, 10$, $Kn = 0$, and $l = 1$. The values presented in this table are limited only to the identical digits out of 10 decimal digits, and they are in perfect agreement. The expansion constants are independent of the Brinkman number, as can be verified from Eqs. (54)-(57).

**Table B.1** The first 10 expansion constants for $Kn = 0$ and $l = 1$.

| $n$ | $Pe = 1$ | | $Pe = 10$ | |
|---|---|---|---|---|
| | $A_n$ | $B_n$ | $A_n$ | $B_n$ |
| 1 | - 0.688950918 | 0.91227178 | - 0.107926367 | 1.37994838 |
| 2 | 0.512563115 | - 0.5511311325 | 0.23283863 | - 0.680026395 |
| 3 | - 0.41657481 | 0.4342973864 | - 0.303512760 | 0.4931037 |
| 4 | 0.359306735 | - 0.37006715 | 0.2966268426 | - 0.406544287 |
| 5 | - 0.3204657258 | 0.327900342 | - 0.279033010 | 0.354039419 |
| 6 | 0.2919526589 | - 0.297490036 | 0.2620290962 | - 0.317633082 |
| 7 | - 0.269889632 | 0.274222535 | - 0.2470098795 | 0.290431052 |
| 8 | 0.2521669185 | - 0.255678113 | 0.2339571532 | - 0.269109882 |
| 9 | - 0.237527822 | 0.240448574 | - 0.22259716 | 0.251824105 |
| 10 | 0.225171708 | - 0.227651188 | 0.212645526 | - 0.237450077 |

Table B.2 shows the comparison between the values of the first 10 expansion constants determined by using Eqs. (54) and (55) with those determined by using Eqs. (56) and (57) for $Kn = 0.01, 0.1$, $Pe = 1$, $\kappa = 1.667$, $\sigma_v = 1$, and $l = 1$. For the downstream region, the results are in perfect agreement. However, for the upstream region, there is a slight change in the values of the first eigenvalues, and this change diminishes after.

**Table B.2** The first 10 expansion constants for $Pe = 1$, $Kn = 0.01,0.1$, $\kappa = 1.667$, $\sigma_v = 1$, and $l = 1$.

| $Kn$ | $n$ | $A_n$ | | $B_n$ | |
|---|---|---|---|---|---|
| | | Equation (54) | Equation (56) | Equation (55) | Equation (57) |
| 0.01 | 1 | - 0.6787224922 | - 0.6858980364 | 0.9168939996 | 0.9168940004 |
| | 2 | 0.5034071553 | 0.5048635919 | - 0.5442560981 | - 0.5442560987 |
| | 3 | - 0.4002482277 | - 0.4009667958 | 0.4199332503 | 0.4199332504 |
| | 4 | 0.3349418823 | 0.3353589599 | - 0.3476465229 | - 0.3476465234 |
| | 5 | - 0.2879090102 | - 0.2881724159 | 0.2972338619 | 0.2972338622 |
| | 6 | 0.2514752005 | 0.2516496329 | - 0.2587938326 | - 0.2587938332 |
| | 7 | - 0.2220303470 | - 0.2221490567 | 0.2279964648 | 0.2279964652 |
| | 8 | 0.1976142200 | 0.1976961689 | - 0.2025901890 | - 0.2025901900 |
| | 9 | - 0.1770318488 | - 0.1770886555 | 0.1812435673 | 0.1812435686 |
| | 10 | 0.1594838978 | 0.1595230498 | - 0.1630855398 | - 0.1630855419 |
| 0.1 | 1 | - 0.4856934128 | - 0.5758467535 | 0.9053770956 | 0.9053770970 |
| | 2 | 0.2936889376 | 0.2851610776 | - 0.3494749162 | - 0.3494749181 |
| | 3 | - 0.1626995917 | - 0.1561907447 | 0.1826308976 | 0.1826308993 |
| | 4 | 0.1038461303 | 0.09895525334 | - 0.1121495548 | - 0.1121495560 |
| | 5 | - 0.07284388737 | - 0.06912105702 | 0.07672136868 | 0.07672137004 |
| | 6 | 0.05447759639 | 0.05155641686 | - 0.05640804108 | - 0.05640804422 |
| | 7 | - 0.04263236294 | - 0.04027351975 | 0.04360875311 | 0.04360875443 |
| | 8 | 0.03449889829 | 0.03254762795 | - 0.03497004720 | - 0.03497004881 |
| | 9 | - 0.02864179952 | - 0.02699527484 | 0.02883025102 | 0.02883025095 |
| | 10 | 0.02426407808 | 0.02285170563 | - 0.02428831908 | - 0.02428831919 |